p-ISSN 1607-6885 New materials and technologies in metallurgy and mechanical engineering. 2026/2
e-ISSN 2786-7358 New materials and technologies in metallurgy and mechanical engineering. 2026/2

UDC 669.721.5:621.785.7

Mykyta Aikin	Senior lecturer of Physical Materials Science Department, National University Zaporizhzhia Polytechnic, Zaporizhzhia, Ukraine, *e-mail: fitone14@gmail.com*, ORCID: 0000-0001-9513-2804
Vadym Shalomeev	Doctor of Technical Sciences, Professor, National University Zaporizhzhia Polytechnic, Zaporizhzhia, Ukraine, *e-mail: shalomeev@zntu.edu.ua*, ORCID: 0000-0002-6091-837X
Yevhen Vyshenko	Student of group IF-213sp, National University Zaporizhzhia Polytechnic, Zaporizhzhia, Ukraine

MICROSTRUCTURE, MECHANICAL PROPERTIES, AND CONTROLLED DEGRADATION OF A BIORESORBABLE MG-3.15ND-1.25ZR-0.6ZN ALLOY FOR OSTEOSYNTHESIS IMPLANTS: INDUSTRIAL PROCESSING AND BENCHMARKING AGAINST ML10 ALLOY

Purpose. *To evaluate the microstructure, mechanical properties, and degradation behaviour of a bioresorbable Mg-3.15Nd-1.25Zr-0.6Zn (wt.%) alloy produced via an industrially compatible route, and to demonstrate its superiority over the reference alloy ML10 for osteosynthesis applications with degradation synchronized to bone healing.*

Research methods. *Microstructure was examined by optical microscopy (Neophot 32, OLYMPUS IX 70) and SEM/EDS (SELMI REM-106I). Grain size was measured by the intercept method (ISO 643:2024). Mechanical properties were determined on an INSTRON 2801 machine (ASTM B557, ISO 6892-1) in the heat-treated condition and after 90-day immersion in Gelofusine (pH 7.4), Venofundin (pH 5.5), and physiological saline at 36 ± 1 °C. Corrosion rates were obtained by gravimetric mass loss. Heat treatment was performed under argon in Bellevue and PAP-4M furnaces. Industrial trials were conducted on malleolar screws of three sizes at JSC "Motor Sich".*

Results. *After casting into a water-cooled copper mould (25–30 °C/s) and two-stage heat treatment (560 °C/8 h + 200 °C/16 h), the alloy exhibited a grain size of 57 ± 4.7 μm (50% finer than ML10), with clean boundaries containing dispersed Zn_2Zr_3 and β″ precipitates instead of continuous $(Mg,Zn)_{12}Nd$ networks. Ultimate tensile strength reached 309 ± 6.5 MPa, yield strength 252 ± 6.5 MPa, and elongation 7.9 ± 0.65% – improvements of 31%, 33%, and 126% over ML10. Corrosion rates (0.45–0.68 mm/year) were 39–42% lower than ML10. After 90 days the alloy retained 58–76% of initial strength (182–230 MPa), maintaining >180 MPa throughout the critical 12-week healing period, versus 38–42% for ML10. Industrial trials on three screw sizes confirmed reproducibility.*

Scientific novelty. *For the first time, a comprehensive evaluation of the interrelationship between microstructure, mechanical properties, and degradation kinetics of the Mg-3.15Nd-1.25Zr-0.6Zn alloy was performed across three model biological fluids with systematic benchmarking against ML10 and bone healing requirements. It was established that elimination of continuous $(Mg,Zn)_{12}Nd$ grain-boundary networks combined with grain refinement to 57 μm shifts the dominant corrosion mode from catastrophic intergranular attack (150–200 μm penetration in ML10) to uniform surface corrosion (<50 μm penetration), yielding degradation kinetics temporally synchronized with the physiological stages of bone healing.*

Practical value. *An industrially scalable route was validated in pilot production of malleolar screws using standard melting, copper-mould casting, and conventional heat treatment. The alloy provides a sufficient mechanical safety margin throughout all critical healing phases (weeks 0–20), surpassing ML10 and meeting preclinical requirements for biodegradable orthopaedic fixation.*

Key words: *biodegradable magnesium alloy, Mg-Zr-Nd-Zn system, osteosynthesis, microstructure, grain refinement, mechanical properties, biocorrosion, controlled degradation, bone healing, malleolar screw, ML10 alloy.*

Introduction

Biodegradable magnesium alloys represent promising candidates for orthopaedic trauma implants by virtue of three key advantages. First, the elastic modulus of magnesium (41–45 GPa) closely approximates that of cortical bone (10–30 GPa), thereby minimizing stress shielding effects. Second, Mg^{2+} ions actively promote osteogenesis. Third, biodegradation obviates the need for secondary surgical intervention to remove the implant.

Despite these advantages, magnesium alloys present critical limitations. In chloride-containing physiological environments, excessive corrosion rates lead to subcutaneous gas cavity formation, localized pH elevation, and premature loss of mechanical integrity prior to completion

DOI 10.15588/1607-6885-2026-2-2

of the 12–16-week bone healing period. The industrial alloy ML10 (known internationally as part of the Mg-Nd-Zr system developed for aerospace applications), despite acceptable initial properties (σ_{UTS} = 230–240 MPa), retains only 40% of its strength after three months owing to a coarse-grained microstructure with heterogeneous secondary phase distribution.

A critical gap exists between the degradation kinetics of current magnesium alloys and the biomechanical requirements of bone healing. An ideal implant should provide maximal support during early-stage healing (weeks 0–6), progressively transfer load to regenerating bone tissue (weeks 6–16), and maintain load-bearing capacity exceeding 180 MPa throughout the critical 12-week period.

The Mg-Zr-Nd-Zn quaternary system offers considerable promise: zirconium provides grain refinement, neodymium enhances corrosion resistance, and zinc contributes solid solution strengthening. Laboratory investigations have achieved ultimate tensile strengths of 300–365 MPa; however, industrial scalability and systematic validation of biodegradation behaviour remain to be demonstrated.

Analysis of research and publications

Over the past two decades, bioresorbable magnesium alloys have emerged as leading candidates for use in trauma and orthopedic implants. Their growing prominence is primarily attributed to three key advantages over conventional inert metallic materials [1–3]:

1. The elastic modulus of magnesium (41–45 GPa) is much closer to that of cortical bone (10–30 GPa), which helps mitigate stress shielding and the consequent resorption of bone tissue.

2. Mg^{2+} ions exhibit osteoconductive properties, supporting bone growth along the implant surface.

3. Their controlled biodegradation eliminates the need for secondary surgical intervention to remove the implant.

In contrast to stainless steel, cobalt-chromium, and titanium alloys – whose stiffness exceeds that of bone by a factor of 4–10 – magnesium alloys preserve a more physiological distribution of mechanical loads within the bone-implant system. This feature is particularly critical in the talar region of the ankle joint, where stress shielding can delay fracture consolidation, reduce bone mineral density, and increase the risk of clinical recurrence.

However, magnesium-based implants also exhibit inherent limitations. In chloride-containing physiological environments, anodic dissolution of magnesium leads to the formation of $Mg(OH)_2$ and molecular hydrogen. When corrosion proceeds too rapidly, this can result in [4, 5]:

1. Subcutaneous gas cavities due to hydrogen accumulation.

2. Local alkalization (elevated pH), which suppresses cellular activity.

3. Premature loss of the implant's mechanical integrity.

Pure magnesium degrades at an excessively high rate: its load-bearing capacity is typically lost before completion of the 12–16-week bone healing phase [5, 6]. Additional challenges include the presence of coarse-grained microstructures, galvanic microcells between the matrix and secondary phases, and a pronounced susceptibility to corrosion fatigue and stress corrosion cracking [4]. Fig. 1 illustrates the critical mismatch between the degradation kinetics of current magnesium alloys and the biomechanical requirements of bone healing. Conventional Mg alloys lose their strength too rapidly, falling below the critical threshold of 180 MPa as early as week 6. The ML10 alloy provides insufficient mechanical support during the crucial phase of hard callus formation, maintaining only 140–160 MPa between weeks 6 and 12. Even the benchmark alloy WE43, although characterized by relatively controlled degradation, exhibits a low initial strength (about 210 MPa) and approaches the critical threshold too closely (183 MPa at week 8), offering an inadequate safety margin.

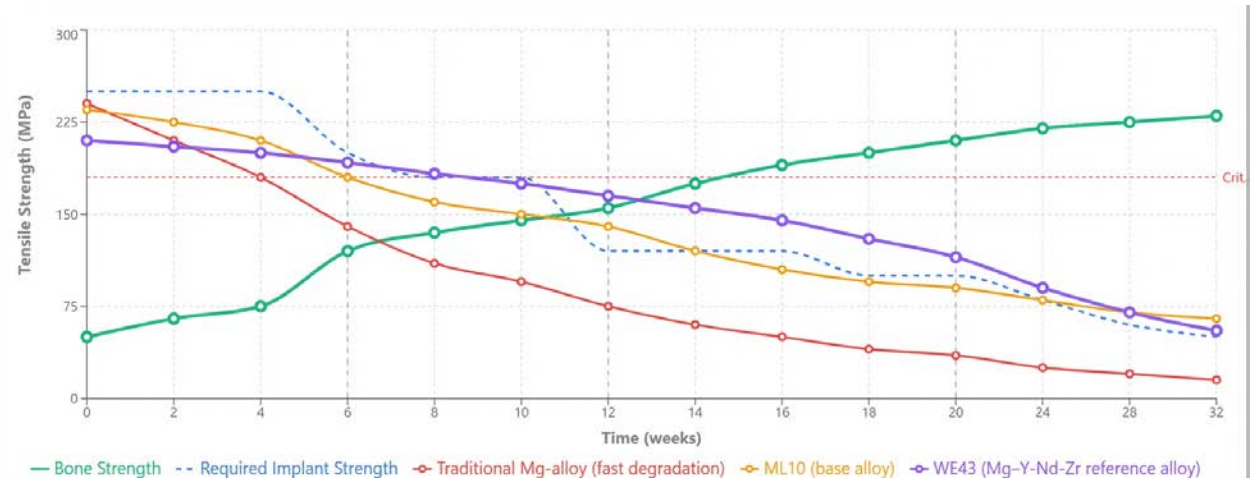

Figure 1. Critical gap in mechanical support: current biodegradable magnesium alloys versus bone healing requirements

DOI 10.15588/1607-6885-2026-2-2

These observations underscore the need to develop a new magnesium alloy with (i) higher initial strength (>250 MPa) and (ii) finely tuned degradation kinetics that are temporally synchronized with the physiological stages of bone tissue regeneration.

Contemporary development of bioresorbable magnesium alloys is centered on three interrelated strategies [3, 5, 7]:

1. Optimizing alloying elements to simultaneously strengthen the matrix and suppress corrosion.
2. Engineering fine-grained, homogeneous microstructures.
3. Designing heat-treatment protocols that homogenize phase distribution and reduce microgalvanic activity without compromising ductility.

The Mg-Zr-Nd-Zn system is particularly promising. Zirconium is the most effective grain refiner in aluminium-free magnesium alloys: it reduces dendritic cell size, promotes a uniform distribution of secondary phases, and improves the isotropy of mechanical properties. Neodymium significantly enhances corrosion resistance and thermal stability while maintaining cytocompatibility. Zinc provides solid-solution strengthening without forming extensive galvanic networks, provided its concentration remains moderate [3, 6, 7]. Experimental studies within this system have already achieved ultimate strengths in the range of 300–365 MPa, combined with acceptable ductility and significantly reduced corrosion rates [1–3]. However, these results have been obtained predominantly at the laboratory scale; industrial scalability, together with standardized validation of biocompatibility and controlled degradation, still require systematic verification.

The industrial reference alloy ML10 exhibits acceptable mechanical properties, but its microstructure is coarse-grained with a non-uniform distribution of large secondary phases. In physiological substitute fluids, this microstructural heterogeneity leads to a more rapid loss of ductility and strength than is desirable for fracture consolidation in the ankle region. Consequently, there remains a clear need for an alloy that [2, 5, 8]:

1. Surpasses ML10 in terms of initial mechanical performance.
2. Maintains critical reserves of strength and ductility throughout the first three months under physiological conditions.
3. Can be reliably produced using standard industrial casting lines.

From a materials science standpoint, microstructural homogeneity and fine grain size are key determinants of corrosion behaviour. Grain refinement enhances the barrier function of grain boundaries, hinders the development of galvanic microcells, and promotes the formation of dense, protective corrosion films. At the same time, excessive dispersion of secondary-phase particles and compositional inhomogeneity can accelerate localized dissolution [3, 5].

Despite encouraging in vitro findings, several critical aspects remain insufficiently documented. It is still unclear to what extent these optimized microstructures can be reliably reproduced under industrial cooling rates and conventional heat-treatment schedules, and whether the mechanical safety margins can be maintained throughout the crucial three-month period in blood-mimicking media. While some studies report ultimate tensile strengths above 300 MPa combined with elongations of 7–10 %, large-scale industrial implementation in actual threaded screw implants remains limited [2, 8].

Standardization of model media is essential. Gelofusine, Venofundin, and physiological saline affect degradation kinetics in distinct ways due to differences in macromolecular and electrolyte composition. Using this spectrum of media enables a more realistic assessment of the time-dependent loss of mechanical properties compared with simpler single-buffer systems [5]. A comprehensive assessment – encompassing initial mechanical properties, microstructural characterization, corrosion dynamics in multiple media, and benchmarking against both cortical bone and the reference alloy ML10 – is consistent with current standards for preclinical validation [3, 8].

The literature points to two parallel trajectories.

The first is scientific and technological: existing studies establish the fundamental feasibility of achieving controlled degradation while retaining high mechanical performance, yet they simultaneously highlight the absence of standardized comparative methodologies and the need for regulatory harmonization [1, 2].

The second is clinical and translational: although preliminary animal and early clinical data support the safety and functional benefits of biodegradable magnesium implants, current evidence is fragmented, dominated by small, heterogeneous cohorts, and often limited to short follow-up periods. This underscores the need for rigorously designed, multicenter studies with unified endpoints (e.g., time to consolidation, complication rates, long-term remodeling of bone and implant remnants), as well as integration of imaging, functional, and patient-reported outcomes to substantiate routine clinical adoption.

Purpose

The aim of this study is to evaluate a bioresorbable Mg-Zr-Nd-Zn alloy that is compatible with standard industrial melting and casting routes, outperforms ML10 in terms of initial mechanical properties, and exhibits controlled degradation in blood-substitute media over a three-month period.

The present study employs a previously developed [8] bioresorbable alloy of composition Mg-1.2…1.3Zr-3.1…3.2Nd-0.5…0.7Zn (wt.%), designed to achieve a synergistic combination of grain refinement (via Zr), corrosion stabilization and dispersion strengthening (via Nd), and solid-solution strengthening (via Zn). The pocessing route was likewise defined on the basis of these earlier investigations [9,10]: melting was carried out in a

DOI 10.15588/1607-6885-2026-2-2

crucible furnace using primary magnesium and master alloys, followed by casting into a water-cooled copper mould (cooling rate 25–30 °C/s). The cast billets were then subjected to a two-step heat treatment consisting of homogenization at 560 ± 5 °C for 8 h with subsequent air cooling, and artificial ageing at 200 ± 5 °C for 16 h.

Industrial trials on ankle screws of three size ranges were conducted to assess the reproducibility of the alloy's microstructure and properties in real components. Degradation behaviour was systematically examined in Gelofusine, Venofundin, and physiological saline, with the loss of strength and ductility quantified after 1, 2, and 3 months of immersion. Comparison with ML10 and with the property range of cortical bone was used to determine whether the alloy retained a sufficient mechanical safety margin to ensure stable fixation throughout the critical healing period [5, 8].

The study demonstrates that an industrially compatible processing route can provide a predictable microstructure and corrosion-mechanical behaviour that meets contemporary preclinical evaluation requirements [1–3]. Successful implementation will provide a foundation for more advanced preclinical studies of biocompatibility and of the systemic effects of degradation products, with a view toward eventual clinical application in the fixation of ankle fractures.

Research material and methodology

Pilot industrial heats of the experimental alloy were carried out in Shop No. 1 of JSC "Motor Sich". Test specimens were manufactured from the new bioresorbable alloy in the form of malleolar screws of different configurations: Type 1 (L = 40 mm, D = 5 mm, d = 3 mm), Type 2 (L = 50 mm, D = 7.5 mm, d = 4.5 mm), and Type 3 (L = 100 mm, D = 7 mm, d = 5.5 mm) (Fig. 2).

The experimental bioresorbable magnesium alloy was developed within the Mg-Zr-Nd-Zn system to balance mechanical strength against biodegradation rate. The target composition comprised 0.4–1.5 wt.% Zr, 2.2–3.4 wt.% Nd, and 0.1–0.7 wt.% Zn. The charge materials consisted of primary ingot magnesium (grades Mg90, Mg95, and Mg96), zinc (grade Ts2), an Mg-Nd master alloy (20–35 wt.% Nd, ≤2.5 wt.% impurities, balance Mg), and an Mg-Zr master alloy (10–20 wt.% Zr, ≤5 wt.% impurities, balance Mg).

Melting was carried out in an IPM-500 crucible furnace (capacity 0.5 t, power 140 kW, throughput 230 kg/h). Preheated charge materials were melted and tapped into removable crucibles at 650–730 °C. The melt was then transferred to holding furnaces, where its composition was adjusted and it was refined with VI-2 flux at 740–760 °C. The VI-2 flux had the following composition: 38–46 wt.% $MgCl_2$, 32–42 wt.% KCl, 5–8 wt.% $BaCl_2$, 3–5 wt.% CaF_2, ≤8 wt.% NaCl + $CaCl_2$, and ≤1.5 wt.% MgO. The Zr-, Nd- and Zn-containing master alloys were then added, and the melt was held at 730 °C prior to casting [11].

For industrial validation, the alloys were cast into water-cooled copper moulds, achieving a cooling rate of 25–30 °C/s. The cooling rate was measured using type-K (Chromel-Alumel) thermocouples, with an operating range from -400 to +1200 °C, positioned in direct contact with the melt.

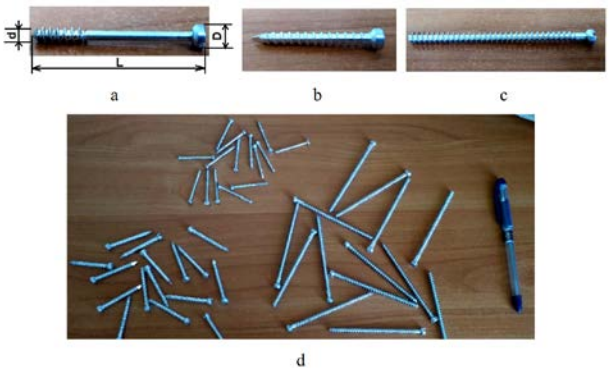

Figure 2. Test specimens of varying length. (a) Type 1; (b) Type 2; (c) Type 3; (d) general view

Heat treatment was carried out in a protective argon atmosphere using either a "Bellevue" pit furnace (112 kW, 95 kg/h) or a PAP-4M furnace (50 kg/h).

The optimized heat-treatment schedule consisted of:

1. Homogenization: 560 ± 5 °C for 8 h, followed by air cooling.

2. Ageing**:** 200 ± 5 °C for 16 h, followed by air cooling.

Optical microscopy. The macro- and microstructure were examined using Neophot 32 and Olympus IX 70 optical microscopes at magnifications of 100×, 200×, 350×, and 500×. Metallographic specimens were prepared after heat treatment and subsequently etched. The etchant composition was: 1 % HNO_3, 20 % CH_3COOH, 19 % distilled water, and 60 % ethylene glycol.

Grain size analysis. The average grain size was determined in accordance with ISO 643:2024 using the intercept method [12]. At 100× magnification, grain boundaries intersected by a test line were counted as following. For each specimen, at least eight representative regions were analysed, with a minimum of two non-parallel measurements per region, each intersecting at least ten grains.

The average grain size D was calculated from:

$$D = L/N, \quad (1)$$

where L is the total length of the test line converted to the image scale (μm), and N is the number of grain boundary intersections along this line.

The standard deviation S was determined as:

$$S = \sqrt{\frac{1}{n}\sum_{i=1}^{n}(D_i - \bar{D})^2}\ , \quad (2)$$

where D_i is the grain size measured in the i-th test, $\bar{D}$ is the arithmetic mean grain size, and n is the number of measurements.

DOI 10.15588/1607-6885-2026-2-2

Ultimate tensile strength and elongation to fracture were determined on an INSTRON 2801 universal testing machine in accordance with ASTM B557 [11] and ISO 6892-1 [13]. Tests were performed both on specimens in the heat-treated condition and after immersion in artificial blood substitutes (Gelofusine, Venofundin, and physiological saline) for 1, 2, and 3 months at 36 ± 1.0 °C [14]. Temperature stability during immersion was maintained using a UT-15 ultra-thermostat.

Specimen preparation. Prior to immersion, the specimens were degreased with ethyl alcohol. After the specified exposure time, the samples were removed and corrosion products were chemically stripped in chromic acid at 18–25 °C for 3 min. The specimens were then rinsed with running water followed by distilled water, dried, and subjected to mechanical testing. For each test condition, three specimens were examined [14].

The compositions of the artificial blood substitutes are summarized in Table 1.

Table 1 – Composition of artificial blood substitutes

Solution	Succinylated gelatin (g/500 mL)	NaCl (g/500 mL)	NaOH (g/500 mL)	Hydroxyethyl starch (g/500 mL)	pH
Gelofusine	20	3,5	0,68	–	7,4
Venofundin	–	4,5	–	30	5,5
Normal saline	–	4,5	–	–	5,5–7,0

Note: Normal saline denotes 0.9% NaCl solution (4.5 g/500 mL).

Specimen quality was assessed by visual inspection and radiographic examination. Visual inspection was used to identify surface defects, damage, and shrinkage cavities, whereas radiographic testing was employed to detect internal defects, porosity, and flux inclusions.

Results and their discussion

The developed Mg-3.15Nd-1.25Zr-0.6Zn alloy exhibited a markedly refined microstructure compared with the reference alloy ML10. Quantitative metallographic analysis revealed an average grain size of 57 ± 4.7 μm, which is approximately 50% smaller than the 115 ± 9.1 μm measured for ML10 (Fig. 3).

Such pronounced grain refinement is consistent with the Hall-Petch relationship, which predicts an improvement in mechanical properties with decreasing grain size [15].

Grain refinement resulted from the synergistic effect of the elevated Zr content (1.25 wt.%) and the optimized heat-treatment parameters. Zirconium acts as a strong grain refiner in magnesium alloys, providing heterogeneous nucleation sites for α-Mg grains during solidification [16]. Differential thermal analysis (DTA) identified the melting temperature of the pseudoeutectic at 571.4 °C, which guided the choice of a homogenization temperature of 560 °C – high enough to ensure complete dissolution of the $(Mg, Zn)_{12}Nd$ eutectic phase while avoiding the risk of incipient melting.

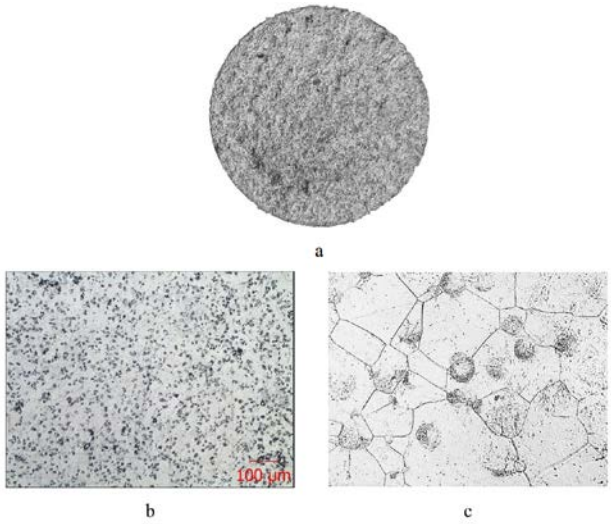

Figure 3. Microstructure of Mg-3.15Nd-1.25Zr-0.6Zn and ML10 alloys. (a) Macrostructure showing uniform grain distribution, ×5; (b) ML10 microstructure with secondary phase particles at grain boundaries, ×100; (c) developed alloy with refined grains and clean boundaries, ×100

The most important microstructural feature of the developed alloy is the presence of clean grain boundaries free from continuous networks of grain-boundary precipitates (Fig. 3*a*). In contrast, ML10 is characterized by extensive decoration of grain boundaries with coarse pseudoeutectic $(Mg, Zn)_{12}Nd$ phases (Fig. 3*b*). These boundary phases act as preferential corrosion sites and stress concentrators [17]. In the developed alloy, the grain boundaries instead contain fine, uniformly distributed Zn_2Zr_3 particles together with metastable β″ secondary-phase precipitates, which provide effective dispersion strengthening without degrading corrosion resistance.

The developed alloy exhibited superior mechanical properties compared with ML10 for all measured parameters (Table 2).

Its ultimate tensile strength of 309 MPa exceeds the threshold typically required for load-bearing orthopaedic applications [18]. More importantly, the yield strength of 252 MPa exceeds the minimum level recommended for osteosynthesis screws in clinical use. The simultaneous improvement in ductility (7.9% elongation compared with 3.5% for ML10) is particularly noteworthy, given that bioresorbable implants are often prone to embrittlement during degradation [17].

These improvements can be attributed to three concurrent strengthening mechanisms:

1. Grain boundary strengthening via the Hall-Petch effect. Grain refinement increases the yield strength in accordance with the Hall-Petch relationship, as the higher grain-boundary area in fine-grained microstructures provides more effective barriers to dislocation motion [15].

DOI 10.15588/1607-6885-2026-2-2

Table 2 – Comparative mechanical properties

Property	Developed alloy	ML10	Improve-ment
Grain size (μm)	57±4,7	115±9,1	−50 %
Ultimate tensile strength (MPa)	309±6,5	235±5,0	+31 %
Yield strength (MPa)	252±6,5	190±5,0	+33 %
Elongation to failure (%)	7,9±0,65	3,5±0,5	+126 %
Residual UTS after 3 months (MPa)	206±24	94±2	+119 %
Strength retention (%)	66±8	40±2	+65 %

2. Solid-solution strengthening. The higher neodymium content (3.15 wt.% vs. 2.5 wt.% in ML10) together with the increased zinc content (0.6 wt.% vs. 0.4 wt.%) markedly contributes to strengthening via lattice distortion. Neodymium has a relatively high solubility in magnesium and, owing to its larger atomic radius, generates significant local lattice strain.

3. Dispersion strengthening. Complete dissolution of the pseudoeutectic during homogenization, followed by controlled ageing, produced a higher volume fraction of fine Zn_2Zr_3 and β″ secondary-phase particles compared with ML10. These coherent or semi-coherent precipitates impede dislocation motion through the Orowan mechanism.

The elimination of coarse secondary-phase particles at grain boundaries also removes preferred crack-initiation sites, which explains the improved ductility. Fractographic analysis revealed predominantly transgranular dimpled fracture in the developed alloy, in contrast to the intergranular brittle fracture observed in ML10, corroborating the beneficial effect of clean grain boundaries on fracture toughness.

Long-term mechanical integrity during degradation represents a critical differentiating factor for bioresorbable orthopaedic implants [19]. The developed alloy retained 58–76 % of its initial strength after three months of immersion in simulated biological fluids – an improvement of 45–90 % relative to the 40% retention observed for ML10 (Fig. 4).

Even under the most aggressive test conditions (Venofundin, pH 5.5), the developed alloy maintained an ultimate tensile strength of 182 ± 18 MPa after 90 days, sufficient for load-bearing function throughout the critical period of ankle fracture consolidation.

This superior property retention can be attributed to two microstructural factors:

First, the absence of continuous secondary-phase particles at grain boundaries eliminates the most aggressive corrosion pathway. In ML10, galvanic couples form between the α-Mg matrix (anode) and $(Mg, Zn)_{12}Nd$ secondary-phase particles (cathode), creating preferential attack channels along grain boundaries [20]. This leads to rapid intergranular corrosion and premature mechanical failure even at modest overall mass loss.

Second, the refined grain structure (57 μm versus 115 μm) paradoxically improves corrosion resistance despite the increased grain boundary area. Finer grains promote more uniform formation of the protective $Mg(OH)_2/MgO$ film and reduce the size of local galvanic cells [21].

Bioresorbable implants *in vivo* are exposed to diverse chemical environments ranging from neutral pH in healthy tissue to acidic conditions at sites of inflammation or hematoma [22]. Table 3 summarizes the corrosion kinetics and evolution of mechanical properties.

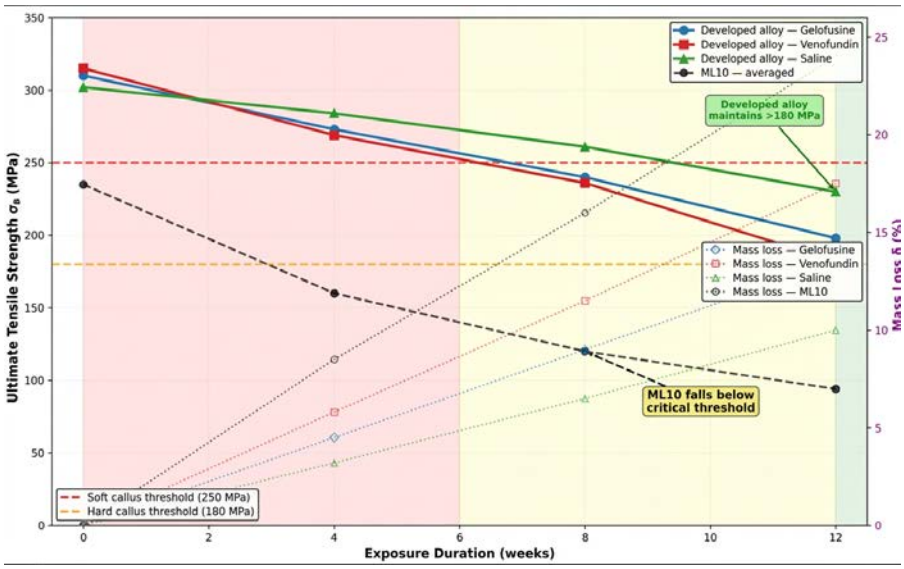

Figure 4. Biaxial plot of ultimate tensile strength retention (MPa) versus time (weeks) for both alloys in all three solutions, with cumulative mass loss (%)

DOI 10.15588/1607-6885-2026-2-2

Table 3 – Degradation characteristics in model biological fluids (90-day immersion)

Solution	CR[a] (mm/year)	Residual UTS (MPa)	Residual El. (%)
Developed Mg–3.15Nd–1.25Zr–0.6Zn			
Gelofusine	0,45±0,05	198±12 (64 %)	5,2±0,8 (65 %)
Normal saline	0,52±0,06	230±15 (76 %)	6,8±1,0 (86 %)
Venofundin	0,68±0,08	182±18 (58 %)	4,0±0,9 (50 %)
ML10			
Gelofusine	0,78±0,08	98±3 (42 %)	1,2±0,2 (40 %)
Normal saline	0,85±0,09	95±2 (40 %)	1,2±0,2 (40 %)
Venofundin	1,12±0,12	89±4 (38 %)	1,1±0,2 (37 %)

Note: [a]Corrosion rate determined by gravimetric mass loss.

Values represent mean ± SD (n = 3). Parenthetical percentages indicate retention relative to initial properties (Table 2). El. = elongation to failure.

The developed alloy consistently exhibited 39–42% lower corrosion rates across all test solutions compared with ML10. This improvement is particularly significant in acidic Venofundin (0.68 mm/year versus 1.12 mm/year for ML10), a 39 % reduction, which simulates the inflammatory microenvironment of early postoperative healing.

Degradation rates varied systematically with solution composition, ranging from slowest in protein-containing Gelofusine (0.45 mm/year), to intermediate in physiological saline (0.52 mm/year), to fastest in acidic Venofundin (0.68 mm/year). This trend reflects three distinct corrosion-modifying mechanisms.

In Gelofusine, albumin and other plasma proteins adsorb onto the magnesium surface, forming a semi-protective organic layer that partially impedes electrolyte access to the underlying metal [22]. For ML10 in this medium, the corrosion rate reached 0.78 mm/year, 73% higher than the experimental alloy, indicating that protein-mediated passivation is less effective on this alloy's surface.

In physiological saline, the absence of proteins eliminates this organic barrier, resulting in moderately accelerated degradation (0.52 mm/year for the developed alloy versus 0.85 mm/year for ML10). Nevertheless, the neutral pH permits rapid formation of a stable $Mg(OH)_2$ layer, which provides partial surface protection.

In acidic Venofundin (pH 5.5), proton reduction becomes the dominant cathodic reaction, accelerating overall corrosion to 0.68 mm/year for the developed alloy and 1.12 mm/year for ML10. Moreover, the acidic environment continuously dissolves the protective $Mg(OH)_2$ layer, preventing the establishment of a stable barrier.

The interrelationship between microstructure, degradation mode, and mechanical property retention is well established in the magnesium alloy literature [20].

Coarse-grained alloys exhibiting extensive secondary phase precipitation along grain boundaries, such as ML10, are susceptible to severe intergranular corrosion, with penetration depths reaching 150–200 μm following prolonged exposure, as the grain boundary networks serve as preferential corrosion pathways. This attack pattern results in catastrophic loss of load-bearing cross-section and premature mechanical failure. In contrast, alloys possessing fine-grained microstructures with homogeneous alloying element distribution exhibit uniform surface corrosion with limited penetration depth (<50 μm), thereby preserving the structural integrity of the bulk material [20].

This difference in corrosion morphology directly accounts for the observed dissolution kinetics in plasma substitute media. Intergranular attack generates internal fissures that act as stress concentrators, inducing brittle fracture at loads substantially below the nominal strength of the residual material, a mechanism consistent with the pronounced strength deterioration of ML10 to 38–42% of initial values across all model solutions. Conversely, uniform surface recession maintains a defect-free cross-section, enabling the material to sustain loads proportional to its remaining cross-sectional area, thus explaining the retention of 58–76% of initial strength in the developed alloy, depending on environmental aggressivity.

The ultimate criterion for success in bioresorbable orthopaedic implants is controlled degradation synchronized with bone healing kinetics. An ideal bioresorbable screw should provide maximal mechanical support during the early healing phase (weeks 0–6), then progressively transfer load to the regenerating bone as it gains strength (weeks 6–16).

Table 4 quantifies the requirements for each healing stage and evaluates both alloys against these benchmarks.

During Phase 1 (weeks 0–6), only a soft fibrous callus with minimal mechanical competence is present at the fracture site; accordingly, the implant must bear virtually 100% of applied loads. Both alloys initially satisfy this requirement, although ML10 affords a narrower safety margin.

The critical distinction emerges in Phase 2 (weeks 6–12), when hard callus formation commences but bone strength remains below 150 MPa. The developed alloy maintains 195–230 MPa throughout this period, sufficient for safe load sharing between implant and healing tissue. In contrast, ML10 degrades to 140–160 MPa, creating a biomechanical mismatch wherein the implant can no longer adequately support applied loads [18].

By Phase 3 (weeks 12–20), the bone has developed sufficient lamellar architecture to assume the majority of loading, requiring only >120 MPa residual strength from the implant. The developed alloy comfortably maintains this threshold (120–180 MPa), whereas ML10 has degraded to 85–95 MPa, below the safety limit.

Phase 4 (weeks 20–32) corresponds to complete bone union, at which point the implant should ideally

DOI 10.15588/1607-6885-2026-2-2

undergo degradation to permit natural bone remodelling. The developed alloy achieves controlled degradation within this timeframe, whereas ML10 frequently fails prematurely.

Table 4 – Healing phase requirements versus alloy performance characteristics

Healing phase	Timeframe	Regenerating bone strength[a]	Implant strength threshold
Healing Phase Requirements			
Inflammation / soft callus	Weeks 0–6	50–80 MPa	>250 MPa
Hard callus formation	Weeks 6–12	120–150 MPa	>180 MPa
Bone remodelling	Weeks 12–20	180–220 MPa	>120 MPa
Complete union	Weeks 20–32	>200 MPa	<100 MPa[c]
Alloy Performance Evaluation			
Healing phase	Developed alloy status	ML10 status	
Inflammation / soft callus	✓ 260–309 MPa	✓ 240–260 MPa[b]	
Hard callus formation	✓ 195–230 MPa	✗ 140–160 MPa	
Bone remodelling	✓ 120–180 MPa	✗ 85–95 MPa	
Complete union	✓ Controlled degradation	✗ Premature failure	

Note: [a]Estimated compressive strength of regenerating fracture callus based on published biomechanical studies.

[b]Marginal compliance; lower-bound values approach threshold.

[c]Upper limit; implant should degrade below this threshold to permit physiological loading of healed bone.

✓ = requirement satisfied; ✗ = requirement not met. Projected implant strengths extrapolated from 90-day immersion data (Table 3).

Conclusions

1. Microstructural achievement. The developed Mg-3.15Nd-1.25Zr-0.6Zn alloy achieved 50% grain refinement (57±4.7 μm versus 115±9.1 μm in ML10) and complete elimination of continuous secondary phase networks at grain boundaries through synergistic effects of elevated Zr content (1.25 wt.%) and optimized two-stage heat treatment (homogenization at 560 °C/8h + ageing at 200 °C/16 h). The resultant microstructure is characterized by clean boundaries with fine, uniformly distributed Zn_2Zr_3 and β" precipitates.

2. Mechanical performance. Ultimate tensile strength of 309±6.5 MPa and elongation of 7.9±0.65% represent improvements of 31% and 126%, respectively, over ML10, while yield strength of 252±6.5 MPa exceeds clinical requirements for load-bearing osteosynthesis screws. These enhancements result from three concurrent strengthening mechanisms: Hall-Petch grain boundary strengthening, solid solution strengthening from Nd and Zn, and Orowan dispersion strengthening from coherent/semi-coherent dispersoids.

3. Controlled degradation synchronized with bone healing. The alloy retained 58–76% of initial strength after three months (depending on solution) versus 38–42% for ML10, maintaining >180 MPa throughout the critical 12-week hard callus formation period across all tested physiological solutions (Gelofusine: 0.45 mm/year; physiological saline: 0.52 mm/year; Venofundin: 0.68 mm/year) – representing a 39–42% reduction in corrosion rate compared with ML10 (0.78–1.12 mm/year). This degradation timeline aligns with bone healing kinetics: adequate support during inflammation/soft callus phases (weeks 0–6), critical load-bearing capacity during hard callus formation (weeks 6–12), and controlled degradation during remodelling (weeks 12–20).

4. Mechanistic understanding. The superior corrosion resistance despite finer grain structure (increased boundary area) results from two interrelated mechanisms: (a) elimination of galvanic corrosion pathways through complete dissolution of anodic $(Mg, Zn)_{12}Nd$ grain boundary networks, and (b) refined grain size promoting uniform protective $Mg(OH)_2/MgO$ film formation while reducing local galvanic cell dimensions. The developed alloy exhibits uniform surface corrosion (<50 μm penetration) versus catastrophic intergranular attack in ML10 (150–200 μm), which accounts for the divergent mechanical property retention despite comparable overall mass loss.

5. Industrial scalability. The processing route: crucible melting, casting into a water-cooled copper mould at 25–30 °C/s, and two-stage heat treatment in standard furnaces, demonstrated reproducible microstructure and properties in industrial trials on threaded malleolar screws of three sizes (Ø3.5, Ø4.0, Ø4.5 mm), confirming compatibility with existing manufacturing infrastructure.

6. Path to clinical translation. Although this study confirms controlled degradation in model biological fluids and biomechanical alignment with bone healing phases, clinical implementation requires: (a) *in vivo* animal studies to evaluate tissue response, hydrogen management, and systemic distribution of degradation products; (b) fatigue property characterization under cyclic physiological loading; (c) evaluation of surface modification strategies (coatings, micro-arc oxidation); and (d) completion of biocompatibility protocols in accordance with ISO 10993 and ASTM F3160.

7. Broader implications. This work demonstrates that rational grain boundary engineering through compositional optimization (Zr modification + Nd stabilization + Zn strengthening) and controlled thermal processing can yield industrially viable biodegradable magnesium alloys with degradation timelines synchronized to tissue healing. The approach is extensible to other temporary load-bearing applications in orthopaedic and cardiovascular devices requiring predictable mechanical support during regeneration followed by controlled resorption.

DOI 10.15588/1607-6885-2026-2-2

References

1. Aikin, M., & Shalomeev, V. (2024). Optimization of heat treatment regime for a new biodegradable Mg-Zr-Nd alloy with enhanced mechanical properties. *Innovative Materials and Technologies in Metallurgy and Mechanical Engineering*, 31–38. https://doi.org/10.15588/1607-6885-2024-3-5

2. Aikin, M., Shalomeev, V., Kukhar, V., Kostryzhev, A., Kuziev, I., Kulynych, V., Dykha, O., Dytyniuk, V., Shapoval, O., & Zagorskis, A. (2025). Recent advances in biodegradable magnesium alloys for medical implants: Evolution, innovations, and clinical translation. *Crystals*, *15*(8), Article 671. https://doi.org/10.3390/cryst15080671

3. Aikin, M., Shalomeev, V., & Lukyanenko, O. (2021). Дослідження впливу високих швидкостей охолодження при кристалізації на структуру та властивості сплаву системи Mg-Zr-Nd [Investigation of the influence of high cooling rates during crystallization on the structure and properties of the Mg-Zr-Nd system alloy]. *Innovative Materials and Technologies in Metallurgy and Mechanical Engineering*. https://doi.org/10.15588/1607-6885-2021-1-4

4. ASTM International. (2004). *Standard guide for laboratory immersion corrosion testing of metals* (ASTM G31-72R04). https://doi.org/10.1520/G0031-72R04

5. ASTM International. (2023). *Standard test methods for tension testing wrought and cast aluminum- and magnesium-alloy products* (ASTM B557-15).

6. Dangwal, S., Edalati, K., Valiev, R. Z., & Langdon, T. G. (2023). Breaks in the Hall-Petch relationship after severe plastic deformation of magnesium, aluminum, copper, and iron. *Crystals*, *13*(3), Article 413. https://doi.org/10.3390/cryst13030413

7. Eddy Jai Poinern, G., Brundavanam, S., & Fawcett, D. (2013). Biomedical magnesium alloys: A review of material properties, surface modifications and potential as a biodegradable orthopaedic implant. *American Journal of Biomedical Engineering*, *2*(6), 218–240. https://doi.org/10.5923/j.ajbe.20120206.02

8. Gracheva, A., Polozov, I., & Popovich, A. (2025). Additive manufacturing of biodegradable metallic implants by selective laser melting: Current research status and application perspectives. *Metals*, *15*(7), Article 754. https://doi.org/10.3390/met15070754

9. International Organization for Standardization. (2019). *Metallic materials-Tensile testing-Part 1: Method of test at room temperature* (ДСТУ ISO 6892-1:2019).

10. International Organization for Standardization. (2024). *Steels-Micrographic determination of the apparent grain size* (ISO 643:2024).

11. Jin, S., Zhang, D., Lu, X., Zhang, Y., Tan, L., Liu, Y., & Wang, Q. (2020). Mechanical properties, biodegradability and cytocompatibility of biodegradable Mg-Zn-Zr-Nd/Y alloys. *Journal of Materials Science & Technology*, *47*, 190–201. https://doi.org/10.1016/j.jmst.2020.02.017

12. Lin, X., Saijilafu, Wu, X., Wu, K., Chen, J., Tan, L., Witte, F., Yang, H., Mantovani, D., & Zhou, H. (2023). Biodegradable Mg-based alloys: Biological implications and restorative opportunities. *International Materials Reviews*, *68*(4), 365–403. https://doi.org/10.1080/09506608.2022.2079367

13. Liu, C., Ren, Z., Xu, Y., Pang, S., Zhao, X., & Zhao, Y. (2018). Biodegradable magnesium alloys developed as bone repair materials: A review. *Scanning*, *2018*, 1–15. https://doi.org/10.1155/2018/9216314

14. Maier, H. J., Julmi, S., Behrens, S., Klose, C., Gartzke, A.-K., Wriggers, P., Waselau, A.-C., & Meyer-Lindenberg, A. (2020). Magnesium alloys for open-pored bioresorbable implants. *JOM*, *72*, 1859–1869. https://doi.org/10.1007/s11837-020-04078-8

15. Morgan, E. F., Unnikrisnan, G. U., & Hussein, A. I. (2018). Bone mechanical properties in healthy and diseased states. *Annual Review of Biomedical Engineering*, *20*, 119–143. https://doi.org/10.1146/annurev-bioeng-062117-121139

16. Müller, E., Schoberwalter, T., Mader, K., Seitz, J.-M., Kopp, A., Baranowsky, A., & Keller, J. (2024). The biological effects of magnesium-based implants on the skeleton and their clinical implications in orthopedic trauma surgery. *Biomaterials Research*, *28*, Article 0122. https://doi.org/10.34133/bmr.0122

17. Shalomeev, V., Aikin, N., Chorniy, V., & Naumik, V. (2019). Design and examination of the new biosoluble casting alloy of the system Mg-Zr-Nd for osteosynthesis. *Materials Science*.

18. Thomas, K. K., Zafar, M. N., Pitt, W. G., & Husseini, G. A. (2023). Biodegradable magnesium alloys for biomedical implants: Properties, challenges, and surface modifications with a focus on orthopedic fixation repair. *Applied Sciences*, *14*(1), Article 10. https://doi.org/10.3390/app14010010

19. Xi, Z., Wu, Y., Xiang, S., Sun, C., Wang, Y., Yu, H., Fu, Y., Wang, X., Yan, J., & Zhao, D. (2020). Corrosion resistance and biocompatibility assessment of a biodegradable hydrothermal-coated Mg-Zn-Ca alloy: An in vitro and in vivo study. *ACS Omega*, *5*, 4548–4557. https://doi.org/10.1021/acsomega.9b03889

20. Yuan, W., Panigrahi, S. K., Su, J.-Q., & Mishra, R. S. (2011). Influence of grain size and texture on Hall-Petch relationship for a magnesium alloy. *Scripta Materialia*, *65*, 994–997. https://doi.org/10.1016/j.scriptamat.2011.08.028

21. Zhang, T., Wang, W., Liu, J., Wang, L., Tang, Y., & Wang, K. (2022). A review on magnesium alloys for biomedical applications. *Frontiers in Bioengineering and Biotechnology*, *10*, Article 953344. https://doi.org/10.3389/fbioe.2022.953344

22. Zhang, X., Yuan, G., Niu, J., Fu, P., & Ding, W. (2012). Microstructure, mechanical properties, biocorrosion behavior, and cytotoxicity of as-extruded Mg-Nd-Zn-Zr alloy with different extrusion ratios. *Journal of the Mechanical Behavior of Biomedical Materials*, *9*, 153–162. https://doi.org/10.1016/j.jmbbm.2012.02.002

Received 12.03.2026
Accepted 20.03.2026
Published 07.05.2026

DOI 10.15588/1607-6885-2026-2-2

УДК 669.721.5:621.785.7

МІКРОСТРУКТУРА, МЕХАНІЧНІ ВЛАСТИВОСТІ ТА КОНТРОЛЬОВАНА ДЕГРАДАЦІЯ БІОРОЗЧИННОГО СПЛАВУ MG-3,15ND-1,25ZR-0,6ZN ДЛЯ ІМПЛАНТІВ ОСТЕОСИНТЕЗУ: ПРОМИСЛОВА ТЕХНОЛОГІЯ ТА ПОРІВНЯЛЬНА ОЦІНКА ЗІ СПЛАВОМ МЛ10

Микита Айкін — старший викладач кафедри фізичного матеріалознавства, Національний університет «Запорізька політехніка», Запоріжжя, Україна, *e-mail: fitone14@gmail.com*, ORCID: 0000-0001-9513-2804

Вадим Шаломєєв — д-р техн. наук, професор, Національний університет «Запорізька політехніка», Запоріжжя, Україна, *e-mail: shalomeev@zntu.edu.ua*, ORCID: 0000-0002-6091-837X

Євген Вишенко — студент групи ІФ-213сп, Національний університет «Запорізька політехніка», Запоріжжя, Україна

Мета. *Оцінити мікроструктуру, механічні властивості та деградаційну поведінку біорозчинного сплаву Mg-3,15Nd-1,25Zr-0,6Zn (мас.%), виготовленого за промислово сумісною технологією, та продемонструвати його переваги над сплавом МЛ10 для остеосинтезу з кінетикою деградації, синхронізованою із загоєнням кістки.*

Методи дослідження. *Мікроструктуру досліджували методами оптичної мікроскопії (Neophot 32, OLYMPUS IX 70) та СЕМ/ЕДС (SELMI PEM-106I). Розмір зерна визначали методом перетинів (ISO 643:2024). Механічні властивості вимірювали на машині INSTRON 2801 (ASTM B557, ISO 6892-1) у термічно обробленому стані та після 90-добової витримки у Гелофузині (pH 7,4), Венофундині (pH 5,5) та фізіологічному розчині при 36 ± 1 °C. Швидкість корозії визначали гравіметричним методом. Термічну обробку проводили в атмосфері аргону у печах Bellevue та ПАП-4М. Промислові випробування виконано на кісточкових гвинтах трьох типорозмірів на АТ «Мотор Січ».*

Результати. *Після лиття у водоохолоджувану мідну виливницю (25–30 °C/с) та двоступеневої термічної обробки (560 °C/8 год + 200 °C/16 год) сплав має розмір зерна 57 ± 4,7 мкм (на 50% менше за МЛ10) з чистими межами, що містять дисперсні частинки Zn_2Zr_3 та β″ замість безперервних мереж $(Mg,Zn)_{12}Nd$. Границя міцності — 309 ± 6,5 МПа, границя текучості – 252 ± 6,5 МПа, подовження – 7,9 ± 0,65%, що на 31%, 33% та 126% вище за МЛ10. Швидкості корозії (0,45–0,68 мм/рік) на 39–42 % нижчі за МЛ10. Після 90 діб сплав зберіг 58–76 % початкової міцності (182–230 МПа), підтримуючи >180 МПа протягом критичного 12-тижневого періоду, проти 38–42 % для МЛ10. Промислові випробування на трьох типорозмірах гвинтів підтвердили відтворюваність.*

Наукова новизна. *Вперше систематично оцінено взаємозв'язок мікроструктури, механічних властивостей та кінетики деградації сплаву Mg-3,15Nd-1,25Zr-0,6Zn у трьох біологічних рідинах із порівнянням з МЛ10 та вимогами загоєння кістки. Встановлено, що усунення міжзеренних мереж $(Mg,Zn)_{12}Nd$ разом із подрібненням зерна до 57 мкм змінює механізм корозії з міжкристалітного (150–200 мкм) на рівномірний поверхневий (<50 мкм), забезпечуючи синхронізацію деградації зі стадіями загоєння.*

Практична цінність. *Промислово масштабовану технологію валідовано у дослідному виробництві кісточкових гвинтів трьох типорозмірів із використанням стандартної тигельної плавки, лиття у мідну виливницю та конвенційної термічної обробки. Сплав забезпечує достатній запас міцності протягом усіх критичних фаз загоєння (тижні 0–20), перевершуючи МЛ10 та відповідаючи доклінічним вимогам до біодеградуючих ортопедичних фіксаторів.*

Ключові слова: *біодеградуючий магнієвий сплав, система Mg-Zr-Nd-Zn, остеосинтез, мікроструктура, механічні властивості, біокорозія, контрольована деградація, загоєння кістки, кісточковий гвинт, сплав МЛ10.*

Список літератури

1. Aikin M., Shalomeev V. Optimization of heat treatment regime for a new biodegradable Mg-Zr-Nd alloy with enhanced mechanical properties. *Innovative Materials and Technologies in Metallurgy and Mechanical Engineering*. 2024. С. 31–38. DOI: https://doi.org/10.15588/1607-6885-2024-3-5

2. Aikin M., Shalomeev V., Kukhar V. et al. Recent advances in biodegradable magnesium alloys for medical implants: evolution, innovations, and clinical translation. *Crystals*. 2025. Vol. 15, № 8. Article 671. DOI: https://doi.org/10.3390/cryst15080671

3. Aikin M., Shalomeev V., Lukyanenko O. Дослідження впливу високих швидкостей охолодження при кристалізації на структуру та властивості сплаву системи Mg-Zr-Nd. Innovative

DOI 10.15588/1607-6885-2026-2-2

Materials and Technologies in Metallurgy and Mechanical Engineering. 2021. DOI: https://doi.org/10.15588/1607-6885-2021-1-4

4. ASTM International. Standard guide for laboratory immersion corrosion testing of metals (ASTM G31-72R04). 2004. DOI: https://doi.org/10.1520/G0031-72R04

5. ASTM International. Standard test methods for tension testing wrought and cast aluminum- and magnesium-alloy products (ASTM B557-15). 2023.

6. Dangwal S., Edalati K., Valiev R. Z., Langdon T. G. Breaks in the Hall-Petch relationship after severe plastic deformation of magnesium, aluminum, copper, and iron. *Crystals*. 2023. Vol. 13, № 3. Article 413. DOI: https://doi.org/10.3390/cryst13030413

7. Poinern G. E. J., Brundavanam S., Fawcett D. Biomedical magnesium alloys: a review of material properties, surface modifications and potential as a biodegradable orthopaedic implant. *American Journal of Biomedical Engineering*. 2013. Vol. 2, № 6. P. 218–240. DOI: https://doi.org/10.5923/j.ajbe.20120206.02

8. Gracheva A., Polozov I., Popovich A. Additive manufacturing of biodegradable metallic implants by selective laser melting: current research status and application perspectives. *Metals*. 2025. Vol. 15, № 7. Article 754. DOI: https://doi.org/10.3390/met15070754

9. Metallic materials. Tensile testing. Part 1: Method of test at room temperature (ДСТУ ISO 6892-1:2019). Київ, 2019.

10. Steels – Micrographic determination of the apparent grain size (ISO 643:2024). 2024.

11. Jin S. та ін. Mechanical properties, biodegradability and cytocompatibility of biodegradable Mg-Zn-Zr-Nd/Y alloys. *Journal of Materials Science & Technology*. 2020. Vol. 47. P. 190–201. DOI: https://doi.org/10.1016/j.jmst.2020.02.017

12. Lin X. та ін. Biodegradable Mg-based alloys: biological implications and restorative opportunities. *International Materials Reviews*. 2023. Vol. 68, № 4. P. 365–403. DOI: https://doi.org/10.1080/09506608.2022.2079367

13. Liu C. та ін. Biodegradable magnesium alloys developed as bone repair materials: a review // Scanning. 2018. Vol. 2018. P. 1–15. DOI: https://doi.org/10.1155/2018/9216314

14. Maier H. J. та ін. Magnesium alloys for open-pored bioresorbable implants. *JOM*. 2020. Vol. 72. P. 1859–1869. DOI: https://doi.org/10.1007/s11837-020-04078-8

15. Morgan E. F., Unnikrisnan G. U., Hussein A. I. Bone mechanical properties in healthy and diseased states. *Annual Review of Biomedical Engineering*. 2018. Vol. 20. P. 119–143. DOI: https://doi.org/10.1146/annurev-bioeng-062117-121139

16. Müller E. et al. The biological effects of magnesium-based implants on the skeleton and their clinical implications in orthopedic trauma surgery. *Biomaterials Research*. 2024. Vol. 28. Article 0122. DOI: https://doi.org/10.34133/bmr.0122

17. Shalomeev V., Aikin N., Chorniy V., Naumik V. Design and examination of the new biosoluble casting alloy of the system Mg-Zr-Nd for osteosynthesis. *Materials Science*. 2019.

18. Thomas K. K. et al. Biodegradable magnesium alloys for biomedical implants: properties, challenges, and surface modifications with a focus on orthopedic fixation repair. *Applied Sciences*. 2023. Vol. 14, № 1. Article 10. DOI: https://doi.org/10.3390/app14010010

19. Xi Z. et al. Corrosion resistance and biocompatibility assessment of a biodegradable hydrothermal-coated Mg-Zn-Ca alloy: an in vitro and in vivo study. *ACS Omega*. 2020. Vol. 5. P. 4548–4557. DOI: https://doi.org/10.1021/acsomega.9b03889

20. Yuan W. та ін. Influence of grain size and texture on Hall-Petch relationship for a magnesium alloy. *Scripta Materialia*. 2011. Vol. 65. P. 994–997. DOI: https://doi.org/10.1016/j.scriptamat.2011.08.028

21. Zhang T. et al. A review on magnesium alloys for biomedical applications. *Frontiers in Bioengineering and Biotechnology*. 2022. Vol. 10. Article 953344. DOI: https://doi.org/10.3389/fbioe.2022.953344

22. Zhang X. et al. Microstructure, mechanical properties, biocorrosion behavior, and cytotoxicity of as-extruded Mg-Nd-Zn-Zr alloy with different extrusion ratios. *Journal of the Mechanical Behavior of Biomedical Materials*. 2012. Vol. 9. P. 153–162. DOI: https://doi.org/10.1016/j.jmbbm.2012.02.002

DOI 10.15588/1607-6885-2026-2-2